内部重力波の傾斜板からの粘性反射

神戸大学 (Kobe University)　片岡　武 (Kataoka, T.)
マサチューセッツ工科大学(MIT) Akylas, T. R.

要旨

We study the effect of viscosity on the 2D reflection of internal gravity wave beams when the Reynolds number is large ($\mathrm{Re} >> 1$). Specifically we make an asymptotic analysis for $\mathrm{Re} >> 1$ to derive a reduced equation describing reflection of wave beam from a sloping boundary. The key is to assume that the beam inclination angle θ and the slope angle α are close to each other so that a reflected beam propagates inside the boundary layer along the slope. Solution of the derived equation agrees well with the corresponding NS solution for $\mathrm{Re} >> 1$.

1. 緒言

Two-dimensional reflection of internal gravity wave beams in a uniformly stratified Boussinesq fluid is considered. Recent laboratory experiments (Gostiaux et al. 2006; Rodenborn et al. 2011; Grisouard et al. 2013) indicate that the beam amplitude is significantly reduced or completely disappear after reflecting from a sloping boundary even when the Reynolds number is large ($\mathrm{Re} >> 1$). Despite such surprising results, there is no systematic analysis that clarifies the effect of viscosity on the reflection of internal wave beams when $\mathrm{Re} >> 1$. In the present study, therefore, we make an asymptotic analysis for $\mathrm{Re} >> 1$ to derive a reduced equation and clarify the effect of viscosity on the above reflection phenomenon.

The key is to assume that the beam inclination angle θ and the slope angle α are close to each other (see figure 1). A reflected beam then has high wavenumber and propagates inside the boundary layer along the slope so that the viscosity can have $O(1)$ effect even when $\mathrm{Re} >> 1$ (Kataoka & Akylas 2020). By taking appropriate scaling we reach a desired equation and solution of this equation is shown to agree well with the corresponding NS solution for $\mathrm{Re} >> 1$.

2. 基礎方程式

Assuming a viscous fluid with kinematic viscosity ν_*, we consider the reflection of internal waves from a rigid slope of constant angle α to the horizontal in an incompressible, uniformly stratified Boussinesq fluid of constant buoyancy frequency N_*. There are no variations along the transverse direction so the flow is two-dimensional. Under these flow conditions, employing a slope-oriented coordinate system with x in the upslope direction and y perpendicular to the slope (see figure 1), the streamfunction $\psi(x,y,t)$ and the reduced density $\rho(x,y,t)$ are governed by the following dimensionless equations derived from the incompressible NS equations:

$$\rho_t + \psi_x \cos\alpha - \psi_y \sin\alpha + J(\rho,\psi) = 0\,, \tag{1a}$$

$$\nabla^2\psi_t - \rho_x \cos\alpha + \rho_y \sin\alpha + J(\nabla^2\psi,\psi) = \nabla^4\psi / \mathrm{Re}\,, \tag{1b}$$

where $J(a,b) = a_x b_y - a_y b_x$ is the Jacobian. To make variables dimensionless, we have used the time scale $1/N^*$ and a characteristic wave length L_* = carrier wavelength $/2\pi$ of the incident wave beam. (Hereafter any constants or variables with asterisk are dimensional, while those

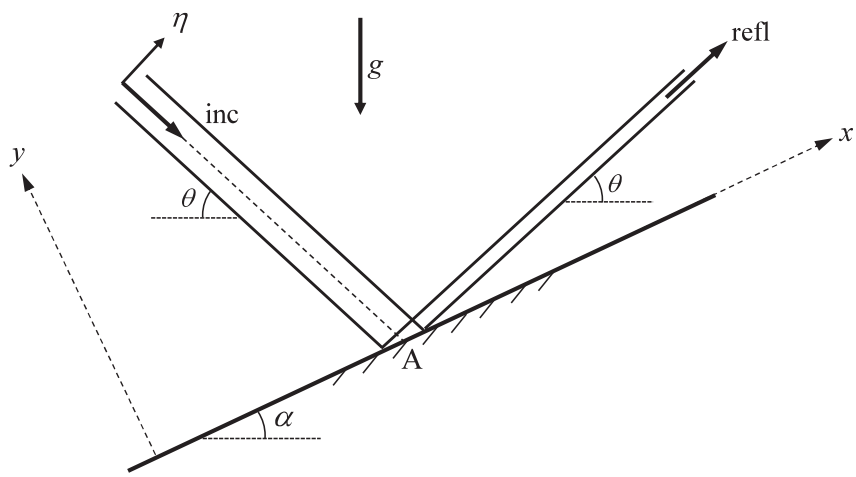

Figure 1. Schematic of reflection of internal wave beam of inclination angle θ from a slope of constant angle α. Reflected wave beam also has an inclination angle θ.

without it are nondimensional). Based on these scales, the Reynolds number is defined as

$$\mathrm{Re} = N_* L_*^2 / \nu_* . \tag{2}$$

Furthermore, for a viscous fluid, the tangential $u = \psi_y$ and the normal $v = -\psi_x$ to the slope velocity components vanish on the slope

$$\psi_x = \psi_y = 0 \quad (y = 0). \tag{3}$$

3. 臨界角近くにおける反射理論

We now develop a weakly nonlinear theory for reflection of internal wave beams of inclination angle θ from the horizontal, accounting for viscous effects when $\mathrm{Re} >> 1$. We introduce the condition of near critical-angle reflection:

$$\alpha = \theta + \sigma\,\mathrm{Re}^{-1/3} \quad (\sigma = O(1)). \tag{4}$$

Equations (1) possess a sinusoidal wave solution of the form $\psi \propto \mathrm{e}^{\mathrm{i}l(x+my)-\mathrm{i}\omega t}$ with $m = \cot(\theta + \alpha)$ and $\omega = \sin\theta$. The incident wave beam can be expressed as a superposition of these sinusoidal waves having the same frequency $\omega = \sin\theta$:

$$\psi^{\mathrm{inc}} = \varepsilon \left\{ Q^{\mathrm{inc}}(x, y)\mathrm{e}^{-\mathrm{i}\omega t} + \mathrm{c.c.} \right\}, \tag{5a}$$

where

$$Q^{\mathrm{inc}}(x, y) = \int_0^\infty \mathrm{d}l A(l) \exp\left\{ \mathrm{i}l(x + my) \right\}. \tag{5b}$$

Here, $A(l)$ is a prescribed function that controls the beam profile and $\varepsilon = U_*^{\mathrm{inc}} / N_* L_* << 1$ is an amplitude parameter that measures nonlinearity, where U_*^{inc} is a maximum velocity of the incident beam.

Turning next to the reflected wave beam, viscosity has an $O(1)$ effect on near-critical reflection, namely when $|\alpha - \theta| \le O(\mathrm{Re}^{-1/3})$ because the inviscid wavenumber normal to the slope becomes large. Under these flow conditions, the reflected disturbance forms an $O(\mathrm{Re}^{-1/3})$ boundary layer next to the slope. Furthermore, when α approaches θ ($|\alpha - \theta| = \varepsilon^{2/3} << 1$) nonlinearity is expected to come into play, too. As a result, the reflected beam again behaves as a boundary layer, whose thickness is $O(\varepsilon^{2/3})$. Thus, at near-critical reflection, nonlinearity and

viscosity are equally important if $\varepsilon^{2/3} = \mathrm{Re}^{-1/3}$, i.e.

$$\varepsilon = \frac{1}{\sqrt{\mathrm{Re}}}. \tag{6}$$

Under the above scaling, we now focus on the boundary layer that forms next to the slope and contains the reflected wave beam. Employing the boundary layer coordinate

$$Y = \mathrm{Re}^{1/3}\, y, \tag{7}$$

$\psi(x,Y,t)$ and $\rho(x,Y,t)$ are expanded as follows:

$$\psi = \frac{1}{\sqrt{\mathrm{Re}}}\left(\psi_1 + \mathrm{Re}^{-1/6}\,\psi_2 + \mathrm{Re}^{-1/3}\,\psi_3 + \cdots\right), \tag{8a}$$

$$\rho = \mathrm{Re}^{-1/6}\, r_1 + \mathrm{Re}^{-1/3}\, r_2 + \mathrm{Re}^{-1/2}\, r_3 + \cdots. \tag{8b}$$

Substituting these expansions in Eqs.(1), to leading order, we obtain

$$\psi_1 = q(x,Y)\mathrm{e}^{-\mathrm{i}\omega t} + \mathrm{c.c.}, \tag{9a}$$

$$r_1 = \mathrm{i}q_Y \mathrm{e}^{-\mathrm{i}\omega t} + \mathrm{c.c.}. \tag{9b}$$

Here, $q(x,Y)$ is the yet undetermined boundary layer profile which must also satisfy the boundary conditions (3) on the slope

$$q_x = q_Y = 0 \quad (Y = 0). \tag{10}$$

In addition, matching of the boundary-layer solution in Eq.(9a) with the incident wave in Eq.(5) at the outer edge of the boundary layer requires that

$$\lim_{Y\to\infty} q = Q^{\mathrm{inc}}(x, y = 0). \tag{11}$$

Proceeding to the next order, from the $O(\mathrm{Re}^{-1/3})$ terms in Eq.(1a) and the $O(1)$ terms in Eq.(1b), along with using Eqs.(10), we find that

$$\psi_2 = \left\{\frac{\mathrm{i}}{\omega}\int_0^Y \mathrm{d}Y' J(q, q_{Y'})\mathrm{e}^{-2\mathrm{i}\omega t} + \mathrm{c.c.}\right\} + \frac{\mathrm{i}}{\omega} J(q, q^*), \tag{12a}$$

$$r_2 = \frac{1}{\omega}\left\{J(q_Y, q)\mathrm{e}^{-2\mathrm{i}\omega t} + J(q, q_Y^*)\right\} + \mathrm{c.c.}. \tag{12b}$$

It should be noted that both the second-harmonic and the mean-flow components of ψ_2 above automatically satisfy the boundary conditions (3) on the slope ($Y = 0$) since q does so according to Eq.(10).

To determine the boundary-layer profile $q(x,Y)$, we return to Eqs.(1) and collect primary-harmonic ($\propto \mathrm{e}^{-\mathrm{i}\omega t}$) terms to the next order. These terms also include contributions from

the interaction of the leading-order disturbance in Eqs.(9) with the induced second-harmonic and mean-flow corrections in Eqs.(12). However, after significant algebra it turns out that these nonlinear (cubic) terms cancel out (Dauxois & Young 1999; Tabaei et al. 2005), leaving the following linear evolution equation for q:

$$\frac{\mathrm{i}}{2\cos\theta} q_{YYYY} + \sigma q_{YY} - q_{xY} = 0 . \tag{13}$$

The boundary conditions are Eqs.(5) and (10). Since this set of equations is linear, we can get the solution explicitly for the incident and the (primary) reflected beam as

$$\psi = \frac{1}{\sqrt{\mathrm{Re}}} Q_1(x,y)\mathrm{e}^{-\mathrm{i}\omega t} + \mathrm{c.c.}, \tag{14a}$$

where

$$Q_1(x,y) = Q^{\mathrm{inc}}(x,y) + \int_0^\infty \mathrm{d}l A(l)\mathrm{e}^{\mathrm{i}lx} \frac{p_1 \exp(\mathrm{i}\,\mathrm{Re}^{1/3}\, p_2 y) - p_2 \exp(\mathrm{i}\,\mathrm{Re}^{1/3}\, p_1 y)}{p_2 - p_1}, \tag{14b}$$

and $p_{1,2}$ are the roots of the cubic equation

$$\frac{\mathrm{i}}{2\cos\theta} p^3 - \sigma p + l = 0 , \tag{15}$$

with $\mathrm{Im}[p_{1,2}] > 0$. Since the leading-order nonlinear terms in Eq.(13) drop out, this linear viscous solution (14) is expected to be also valid for small but finite-amplitude beam.

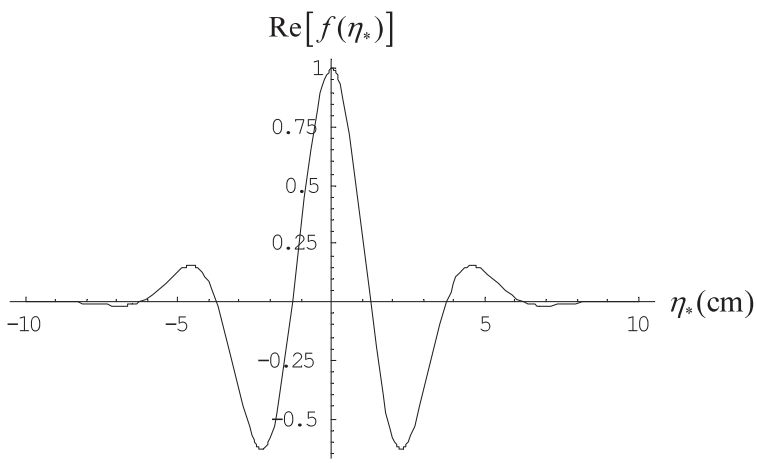

Figure 2. Profile of $\mathrm{Re}\left[f(\eta_*)\right]$ in (16) for $D_* = 3\mathrm{cm}$ and $L_* = 5\mathrm{cm}/2\pi$.

4. 結果

We now apply our theoretical model to an incident wave beam whose velocity profile along the beam consists of a sinusoid with wavelength $2\pi L_*$ multiplied by the Gaussian envelop $\exp[-(\eta_* / D_*)^2]$ as

$$-u_* \cos(\theta+\alpha) + v_* \sin(\theta+\alpha) = \frac{U_*^{\mathrm{inc}}}{2} f(\eta_*) \mathrm{e}^{-\mathrm{i}\omega t} + \mathrm{c.c.}, \tag{16a}$$

where

$$f(\eta_*) = \exp\left[-\left(\frac{\eta_*}{D_*} \right)^2 + \mathrm{i} \frac{\eta_*}{L_*} \right], \tag{16b}$$

(see figure 2 for $f(\eta_*)$) and η_* denotes the across-beam coordinate. This profile with $D_* = 3.5\mathrm{cm}$ and $L_* = 5\mathrm{cm}/2\pi$ mimics the one generated in the laboratory experiment by Rodenborn et al. (2011) which leads to $\mathrm{Re} = 100$ when $N_* = 1.6(\mathrm{rad/s})$. The corresponding $A(l)$ in (5b) is given by $A(l) = \exp\{-[0.35(5l/\sin(\theta+\alpha) - 2\pi)]^2\}/2\pi l$.

For comparison against the theoretical predictions, we also conducted numerical simulations based on the Navier-Stokes equations subject to no-slip conditions on the slope as in Eq.(3), and with a suitable forcing term added on the right-hand side of the momentum equation to drive the incident wave. The numerical solution procedure is similar to the MAC method. The computational domain is taken to be wide enough ($-300\mathrm{cm} < x_* < 300\mathrm{cm}$, $0 < y_* < 100\mathrm{cm}$) such that artificial reflections at the boundaries do not interfere with the beam reflection from the slope during the computation. Furthermore, to improve resolution, grid points (typically 600×600 in $x \times y$) are spaced unevenly, with higher concentration in the overlap region of the incident and the reflected waves and in the boundary layer along the slope. The computation is continued until steady state is reached to a reasonable approximation, which typically takes $20-30$ wave beam periods.

Comparison of NS computational results and our theory is shown in figure 3 for the x_*-velocity fields of reflecting internal wave beams at $\mathrm{Re} = 100$ and $\theta = 22.7^\circ$. These particular Re and θ are also used for the majority of the experimental results reported in Rodenborn et al. (2011). The reflected beam weakens significantly as α approaches $\theta (= 22.7^\circ)$, as the snapshots in these figures illustrate, and almost no wave can be detected for

α close to θ, specifically for $20^\circ \le \alpha \le 28^\circ$. The results of NS computation and our theory agree well for the whole range of α despite the fact that the theory assumes near critical-angle reflection (4).

Figure 4 shows plots, for different Re and ε, of the amplitude of the primary-harmonic reflected beam U_*^{refl} (normalized with the incident beam amplitude U_*^{inc}) at fixed angle of incidence $\theta = 22.7^\circ$, as the slope angle α is varied in the range $0 \le \alpha \le 50^\circ$. U_*^{refl} is defined as the maximum velocity of the reflected beam at 20cm from the reflection point A (see figure1). For the parameter value $\text{Re} = 100$, the viscous solution for the primary reflected beam in Eqs.(14) is in satisfactory agreement with the numerical simulations. Under these flow

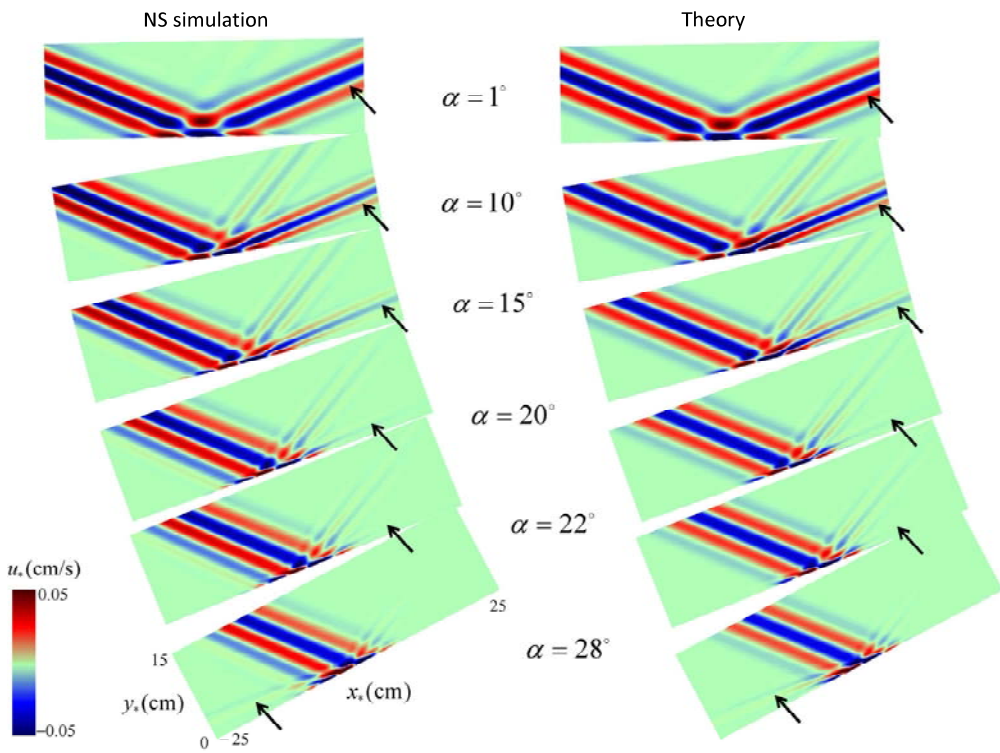

Figure 3 Comparison of NS simulation results (left column) and our theory (right column) for the x_*-velocity fields of beam reflection at fixed $\theta = 22.7^\circ$ and $\text{Re} = 100$. The incident beam profile is (16) with $U_*^{\text{inc}} = 0.05\text{cm/s}$, $D_* = 3.5\text{cm}$ and $L_* = 5\text{cm}/2\pi$. From top, $\alpha = 1^\circ$, 10°, 15°, 20°, 22°, and 28°. The primary-harmonic reflected beams are denoted by the black arrows.

conditions, viscous effects have a dominant role throughout: the resonance peak at the critical slope angle $\alpha = \theta$ predicted by the inviscid theory ($\mathrm{Re} = \infty$) is completely suppressed. The major controlling factor of the response is Re, as illustrated in figure 4 for $\mathrm{Re} = 1000$. In this instance, we also find reasonable agreement between theory and simulation. However, while viscous effects again dominate near $\alpha = \theta$, the response now follows closely the inviscid result for $0 \le \alpha \le 7^\circ$ and features a relatively sharp peak around $\alpha = 12^\circ$. As Re is further increased so viscous effects become less important, the range of α where inviscid theory holds is expected to expand. In addition, the response peak will be steeper and occur closer to, but never reach, the critical angle $\alpha = \theta$, where viscosity cannot be ignored.

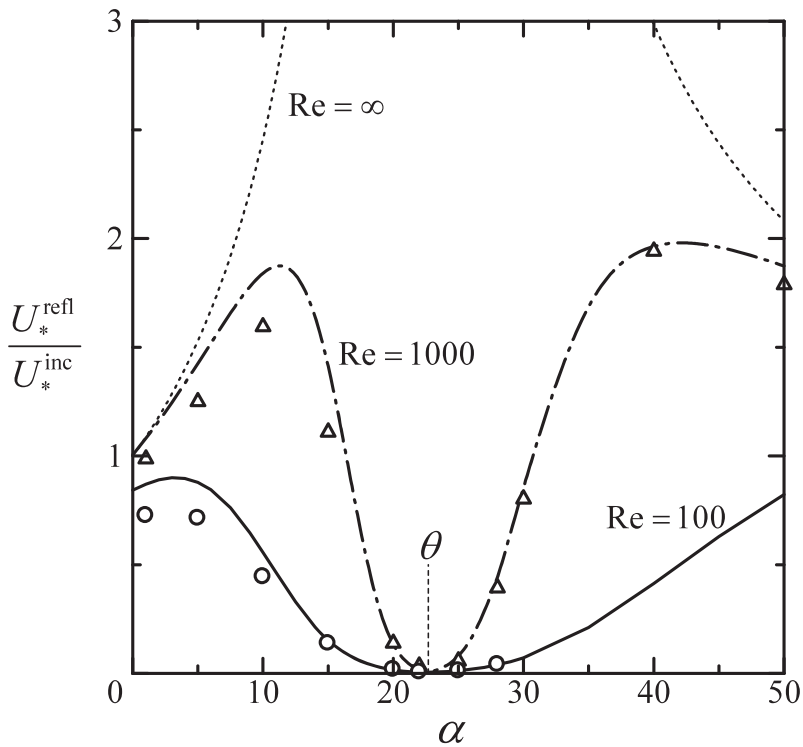

Figure 4 Ratio of reflected beam amplitude to incident beam amplitude $U_*^{\mathrm{refl}} / U_*^{\mathrm{inc}}$ versus α for $\theta = 22.7^\circ$. The solid, dash-dot, and dotted lines are the theoretical results for Re =100, 1000 and ∞, respectively. The points are NS simulation results (○: Re=100, △: Re=1000).

5. 考察と結言

According to Eq.(4), inviscid analysis provides a good approximation for $\mathrm{Re} >> 1$, only if the condition

$$|\theta - \alpha| >> \mathrm{Re}^{-1/3}, \tag{17}$$

is met. Thus, there is a range of incidence angles near the critical $\theta = \alpha$ for which viscous effects cannot be ignored as figure 4 indicates. For the experimental setup of Rodenborn et al. (2011) in particular, $\mathrm{Re} = 100$ so $\mathrm{Re}^{1/3} = 4.6$ and $\mathrm{Re}^{-1/3} = 0.22$. Furthermore, in these experiments, the slope angle was varied in the range $0 \le \alpha \le \theta$ for $\theta = 22.7^\circ$, so $|\alpha - \theta| \le 0.4$ rad. Under these flow conditions, as the inviscid criterion (17) is met rather marginally even at the lower extreme $\alpha = 0$, viscous effects are likely to be important throughout the slope range $0 \le \alpha \le \theta$. This claim is supported by the above theoretical results and numerical simulations presented in Section 4.

The present study treats 2D reflection of the internal wave beam and has focused on the primary-harmonic beam ($\sim e^{-i\omega t}$). It is also worth examining the 2nd-harmonic beam ($\sim e^{-2i\omega t}$) which is produced by interaction of the incident and reflected primary-harmonic beams (Kataoka & Akylas 2020). It is also interesting to look into 3D reflection where the incident beam is oblique, that is, the beam planes of constant phase meet the slope at an arbitrary direction, not necessarily parallel to the isobaths (Dunkerton et al. 1998; Kataoka & Akylas 2019). This 3D reflection will be associated with production of relatively strong mean flow which is called ‘streaming’. We are interested in how strong this mean flow is and how it will feedback to the beam reflection phenomenon as a future work.

参考文献

Dauxois, T., Young, W. R., “Near-critical reflection of internal waves,” *J. Fluid Mech.* **390** (1999), pp. 271–295.

Dunkerton, T. J., Delisi, D. P., Lelong, M-. P., “Alongslope current generated by obliquely incident internal gravity waves,” *Geophys. Res. Lett.* **25** (1998), pp. 3871–3874.

Gostiaux, L., Dauxois, T., Didelle, H., Sommeria, J., Viboud, S., “Quantitative laboratory observations of internal wave reflection on ascending slopes,” *Phys. Fluids* **18** (2006), 056602.

Grisouard, N., Leclair, M., Gostiaux, L., Staquet, C., “Large scale energy transfer from an internal gravity wave reflecting on a simple slope,” *Proc. IUTAM* 8 (2013), pp.

119–128.

Kataoka, T., Akylas, T. R., “On mean flow generation due to oblique reflection of internal waves at a slope,” *Stud. Appl. Math*. **142** (2019), pp. 419–432.

Kataoka, T., Akylas, T. R., “Viscous reflection of internal waves from a slope,” *Phys. Rev. Fluids*. **5** (2020), 014803.

Tabaei, A., Akylas, T. R., Lamb, K. G., “Nonlinear effects in reflecting and colliding internal wave beams,” *J. Fluid Mech.* **526** (2005), pp. 217–243.